RESEARCH ARTICLE | APRIL 08 2025

Double-layer capacitance peaks: Origins, ion dependence, and temperature effects

Special Collection: Yijing Yan Festschrift

Erfei Zhen; Yanxia Chen ; Jun Huang

J. Chem. Phys. 162, 144702 (2025)
https://doi.org/10.1063/5.0251548

The Journal of Chemical Physics ARTICLE pubs.aip.org/aip/jcp

Double-layer capacitance peaks: Origins, ion dependence, and temperature effects

Cite as: J. Chem. Phys. 162, 144702 (2025); doi: 10.1063/5.0251548
Submitted: 3 December 2024 • Accepted: 17 March 2025 •
Published Online: 8 April 2025

Erfei Zhen,[1] Yanxia Chen,[1,a)] and Jun Huang[2,3,a)]

AFFILIATIONS

[1] Hefei National Research Center for Physical Sciences at Microscale, Department of Chemical Physics, University of Science and Technology of China, Hefei 230026, China
[2] Institute of Energy Technologies, IET-3: Theory and Computation of Energy Materials, Forschungszentrum Jülich GmbH, 52425 Jülich, Germany
[3] Theory of Electrocatalytic Interfaces, Faculty of Georesources and Materials Engineering, RWTH Aachen University, Aachen 52062, Germany

Note: This paper is part of the Special Topic, Yijing Yan Festschrift.
[a)] **Authors to whom correspondence should be addressed:** yachen@ustc.edu.cn and ju.huang@fz-juelich.de

ABSTRACT

Differential capacitance (C_{dl}) is arguably the most important lumped parameter of electrical double layers (EDLs). Two peaks in the C_{dl} profile have been commonly attributed to the crowding of counterions within the EDL. More recent studies have suggested that the two peaks are primarily caused by orientational polarization of interfacial water molecules. Herein, this recent perspective is extended by considering orientation-dependent adsorption free energy of water and tested at Au(111)–aqueous solution interfaces. Our comparative analysis of the ion dependency of the C_{dl} profile corroborates the view that the capacitance peaks are caused mainly by the saturation of the orientational polarization of interfacial water molecules. In addition, the temperature dependency of the C_{dl} profile is consistently interpreted as a consequence of the temperature effects on the orientational polarization of interfacial water.

I. INTRODUCTION

The electrical double layer (EDL) is a fundamental concept describing the charge separation at the electrified interfaces.[1–5] In a modelistic picture, the EDL comprises two layers, a compact layer of adsorbed solvent molecules and ions, and a diffuse layer with ion distributions dictated by electrostatic and thermal forces.[6] Understanding the EDL is essential for optimizing the performance of electrochemical devices such as supercapacitors and fuel cells.[7,8] Central to understanding the EDL is its differential double-layer capacitance (C_{dl}), which has been extensively used as the quintessential property of the structure and dynamics of the EDL.[9–18] As regards mercury and "simple" solid metals (e.g., Au, Ag), the C_{dl} curves often exhibit a pronounced minimum at the potential of zero free charge (pzfc) in dilute electrolyte solutions. As the electrode potential deviates away from the pzfc, C_{dl} quickly increases and then decreases, delineating a distinctive camel-like profile. As electrolyte concentrations increase, the two peaks converge and ultimately merge into a single peak, resulting in a bell-shaped C_{dl} profile.[19–23]

Several explanations have been put forward regarding the two distinct peaks of the camel-shaped C_{dl} curves. We note that the "peaks" discussed in this work should be distinguished from the peak of bell-shaped (Helmholtz) capacitance near the pzfc, as investigated in Refs. 13 and 24.

In the prevailing view, the two C_{dl} peaks are associated with ion overcrowding within the EDL.[25–27] Ion overcrowding effectively increases the thickness of the EDL and decreases C_{dl}. This mechanism has been incorporated into implicit solvation models of EDLs; for instance, Nattino *et al.*[27] adopted a size-modified Poisson–Boltzmann (MPB) model with a maximum local ion concentration (c_{max}) to account for steric repulsion between solvated ions. They used a value of 2M for c_{max}, which is arguably too small, in order to fit the camel-shaped C_{dl} curves observed experimentally for Ag(100)–aqueous interfaces. As the electrode potential is biased

beyond ±0.3 V relative to the pzfc, the counterion density saturates at c_{max} near the electrode surface. The concentration plateau is wider at larger potential bias, effectively increasing the thickness of the EDL and decreasing C_{dl}.

According to this widely held view, variations in ion size should directly influence the potential and magnitude of the two camel-shaped C_{dl} peaks. However, emerging experimental evidence reveals inconsistencies with this paradigm. Studies at the Au(111) electrodes–aqueous solutions have shown that the C_{dl} peak on the negative side is identical within the experimental error for different alkali metal cations (Li^+, Na^+, and K^+).[28] Moreover, it is expected that the smaller the ionic hydration diameter, the higher the peak of C_{dl} curves. Nonetheless, in a 1 mM $HClO_4$ solution, the experimental C_{dl} curves of the Au(111) exhibit a smaller cathodic peak than that of the anodic peak.[23,29] This contradicts the expectation based on the diameters of the hydronium (5.6 Å) and the hydrated perchlorate ion (6.76 Å).[30] Similarly, Ag(111)–KPF_6 interfaces show symmetric C_{dl} peaks despite the size asymmetry between K^+ (~5.0 Å) and PF_6^- (~4.0 Å).[31,32] These anomalies suggest new underlying factors, other than the overcrowding of counterions, for the C_{dl} peaks.

Schwarz and Sundararaman proposed an alternative view[33,34] that the hump in the C_{dl} curves of the Ag(100)–KPF_6 solution interface is related to the nonlinear dielectric response of water, which was studied first by Booth[35] and more recently by Abrashkin *et al.*[36] and Gunceler *et al.*[37] The key idea involves the saturation of orientational polarization of water molecules induced by the strong local electric field near the electrode surface. The dielectric saturation reduces the local dielectric constant from its bulk value of ~78.5 to below 20 at potential deviating by ±0.2 V from the pzfc within 2–3 Å of the compact layer, thereby suppressing C_{dl} at electrode potentials far away from the pzfc.[33]

Currently, the origin of the double-layer peaks, ion overcrowding, or saturation of orientational polarization of water, is a topic of debate. Herein, we address this open question by using a refined model that incorporates the orientational polarization of the first-layer water molecules, the asymmetric steric effects of ions, and a field-dependent dielectric "constant" of water. This model is parameterized using experimental data and *ab initio* molecular dynamics (AIMD) simulations on Au(111)–aqueous interfaces taken from the literature. Then, the parameterized model is used to investigate the origins of the C_{dl} peaks, their dependence on ion species, and the impact of temperature.

II. MODEL DEVELOPMENT

A. A continuum model for the EDL

A schematic illustration of the continuum EDL model for the Au(111)/electrolyte interface is exhibited in Fig. 1(a). The Au(111) electrode is assumed to be ideally planar. The inner layer is divided into two parts. One is a closest approach plane (CAP), donating the inner plane of the first-layer water molecules closest to the electrode surface.[15] The other is an adsorbed solvent plane (ASP), donating the outer plane of adsorbed water molecules. The water molecules in the first layer are typically strongly polarized, owing to the strong interfacial electric field and chemical interactions with the metal surface.[38] More generally, such refinements can take into account the dielectric environments experienced by the adsorbed water molecules.[17,39]

In the space between the metal surface and the ASP, some water molecules are closer to the Au(111), corresponding to the chemisorbed water found in AIMD simulation. The other water molecules are more distant from the metal, representing the physisorbed water, as shown in Fig. 1(a). Le *et al.* revealed a higher coverage of chemisorbed water at more positive potentials and further related this to the capacitance peak observed on Pt(111)–aqueous solution interfaces.[13,16] It is noted that our model does not distinguish the coverages of different water states; instead, it assumes a constant total coverage of all chemisorbed and

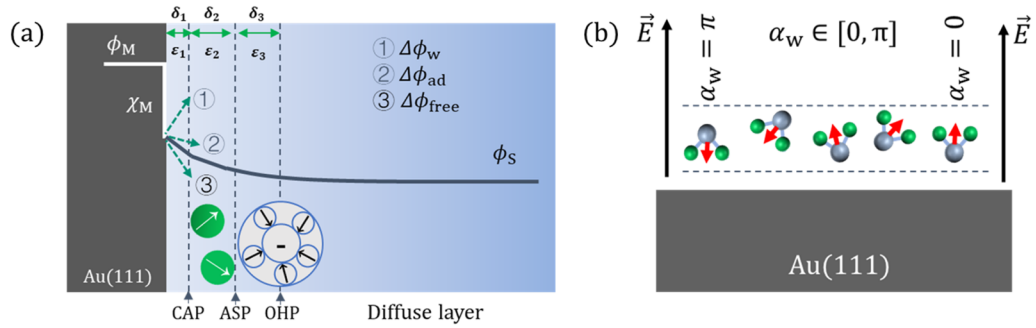

FIG. 1. (a) Continuum model for the EDL at the Au(111)/electrolyte interface, consisting of the closest approach plane (CAP), donating the inner plane of the first-layer water molecules closest to the electrode surface, an adsorbed solvent plane (ASP) donating the outer plane of adsorbed water molecules, and an outer Helmholtz plane (OHP) denoting the central plane of nonspecifically adsorbed ions. The regions between the electrode surface and the CAP, the CAP and the ASP, and the ASP and the OHP are described as dielectric continua, parameterized with respective thicknesses δ_1, δ_2, and δ_3, and dielectric permittivities ε_1, ε_2, and ε_3. (b) A schematic illustration of first-layer water model within the ASP with a continuous spectrum of orientational states. Closer to the electrode surface might be referred to as chemisorbed water and slightly further away from the electrode surface physisorbed water. α_w denotes the angle between water dipoles and the local electric field. α_w can take any values between 0 and π. In this context, the dipole orientation is defined from its negative to its positive end. $\delta\mu$ represents the difference in chemical interaction energy between the scenarios where α_w equals 0 and where α_w equals π, formulated by $\delta\mu = \Delta G_w(\alpha_w = 0) - \Delta G_w(\alpha_w = \pi)$.

physisorbed water molecules within the ASP. At least for C_{dl} curves, our simplified treatment is shown to be sufficient.

Nonspecifically adsorbed ions, such as hydrated H^+, K^+, and ClO_4^-, along with their solvation shell, reside in the diffuse layer that extends from the outer Helmholtz plane (OHP) toward the electrolyte bulk. The regions between the electrode surface and the CAP, the CAP and the ASP, and the ASP and the OHP, are described as dielectric continua, parameterized with respective thicknesses δ_1, δ_2, and δ_3, and permittivities ε_1, ε_2, and ε_3.

B. Decomposition of the electric potential difference

The relationship between the free surface charge (σ_{free}) and the electrode potential (E), named the surface charging relation ($\sigma_{free} - E$), is an informative property of the EDL.[40] To obtain the $\sigma_{free} - E$ relationships, the potential distribution extending from the Au(111) electrode surface to the bulk solution should be determined. The total potential difference between the Au(111) electrode and the solution bulk comprises four elements, as shown in Fig. 1(a) χ_M is the potential drop at the metal–aqueous solution interface, due to electron spillover;[41] $\Delta\phi_w$ is the potential change caused by the orientational polarization of adsorbed water molecules; $\Delta\phi_{ad}$ is the potential change due to partially charged and chemisorbed ions;[40] and $\Delta\phi_{free}$ is the potential change as a result of excess ionic charge accumulated in the diffuse layer. The above-mentioned decomposition is expressed as

$$\phi_M - \phi_S = \chi_M + \Delta\phi_{free} + \Delta\phi_w + \Delta\phi_{ad}. \tag{1}$$

In the present study, the electrolyte ions (H^+, Li^+, Na^+, K^+, ClO_4^-) do not adsorb specifically on the Au(111) surface. After safely neglecting the $\Delta\phi_{ad}$ term in the present case, we simplify Eq. (1) to

$$\phi_M - \phi_S = \chi_M + \Delta\phi_{free} + \Delta\phi_w. \tag{2}$$

As for metals, χ_M is often viewed as a constant independent of ϕ_M.[42,43] In a continuum picture, $\Delta\phi_{free}$ is expressed as

$$\Delta\phi_{free} = \sigma_{free}\left(\frac{\delta_1}{\varepsilon_1} + \frac{\delta_2}{\varepsilon_2} + \frac{\delta_3}{\varepsilon_3}\right) + \Delta\phi_{OHP}^S, \tag{3}$$

where $\Delta\phi_{OHP}^S = \phi_{OHP} - \phi_S$, with ϕ_{OHP} being the potential at the OHP, which is to be calculated in the section of the diffuse layer model. The term $\Delta\phi_w$ in Eq. (2) represents the potential difference, resulted from the average dipole moment of the water molecules in the first layer,

$$\Delta\phi_w = -\frac{N_{ad}\theta_w\mu_w\langle\cos\alpha_w\rangle}{\varepsilon_2}, \tag{4}$$

where N_{ad} is the number density of adsorption sites, θ_w is the coverage of water molecules at the ASP, and μ_w is the intrinsic dipole moment of a water molecules. $\langle\cos\alpha_w\rangle$ represents the statistical average of $\cos\alpha_w$, where α_w denotes the angle between water dipoles and the outward electric field, as illustrated in Fig. 1(b). In this context, the dipole orientation is defined from the negative to positive end of a dipole. A statistical analysis of interfacial water molecules at the ASP (see the supplementary material for a detailed derivation) gives

$$\langle\cos\alpha_w\rangle = -\coth\left(\frac{\mu_w E_{loc} + \delta\mu}{kT}\right) + \frac{kT}{\mu_w E_{loc} + \delta\mu}, \tag{5}$$

where k is the Boltzmann constant and T is the temperature. E_{loc} is the local electric field, calculated as $E_{loc} = -\sigma_{free}/\varepsilon_2$. $\delta\mu$ represents the difference in the chemical energy of water with $\alpha_w = 0$ and that of water with $\alpha_w = \pi$, namely, $\delta\mu = \Delta G_w(\alpha_w = 0) - \Delta G_w(\alpha_w = \pi)$, with ΔG_w being adsorption free energy of interfacial water molecules. $\delta\mu$ accounts for the chemical interactions between water molecules and the metal surface. If $\delta\mu < 0$, water molecules prefer the O-down configuration, otherwise water molecules prefer the H-down configuration.

C. Diffuse layer model

To understand the C_{dl} peaks, the diffuse layer model should, at least, consider asymmetric steric effects of ions and field-dependent permittivity of solvent. Herein, we adopt a mean field model to consider both effects. The Helmholtz free energy per unit volume of the electrolyte solution is expressed as[44,45]

$$f_H = e_0\phi(n_c - n_a) - \frac{\varepsilon_\infty(\nabla\phi)^2}{2} - \frac{1}{\beta}n_s\ln\left(\frac{\sinh\left(\mu_w^{eff}\beta\nabla\phi\right)}{\mu_w^{eff}\beta\nabla\phi}\right) + \frac{1}{\beta}\ln\left(\frac{n!}{n_c!n_a!n_s!}\right), \tag{6}$$

where e_0 is the elementary charge, ε_∞ is the optical permittivity, and μ_w^{eff} is the effective dipole moment of water molecules. We use a different dipole moment for the water molecules in the first layer above the metal surface [μ_w in Eq. (5)] and those in the bulk solution [μ_w^{eff} in Eq. (6)]. This distinction accounts for the different structural symmetries at the interface and in the bulk solution: the first-layer water resembles more isolated molecules with less interconnection, while bulk water enjoys isotropic interactions in a hydrogen bond network. $\beta = \frac{1}{kT}$ is the inverse thermal energy. n_c, n_a, and n_s are the number densities of cations, anions, and solvent molecules, respectively. n is the total number density of lattice sites, that is, $n = \sum_{i=a,c,s}\gamma_i n_i$, with $\gamma_i = \left(\frac{d_i}{d_s}\right)^3$ being the relative size of electrolyte component i referenced to the size of lattice. d_i is the effective diameters of component i. d_s refers to the diameter of solvent molecules, and it serves as the reference size. On the right-hand side of Eq. (6), the first term is the electrostatic free energy of ions. The second term is the self-energy of the electric field. The third term is the electrostatic free energy associated with solvent molecules. The last term is the entropic free energy linked to the configuration of species within the solution, determined through a lattice-gas method.[44]

A variational analysis of Eq. (6) leads to the modified Poisson–Boltzmann equation,

$$-\nabla\cdot(\varepsilon_{eff}\nabla\phi) = e_0(n_c - n_a), \tag{7}$$

with an effective dielectric permittivity,

$$\varepsilon_{\text{eff}} = \varepsilon_{\infty} + \frac{\mu_{\text{w}}^{\text{eff}} n_{\text{s}}}{|\nabla\phi|}\left[\coth\left(\mu_{\text{w}}^{\text{eff}}\beta|\nabla\phi|\right) - \frac{1}{\mu_{\text{w}}^{\text{eff}}\beta|\nabla\phi|}\right]. \tag{8}$$

In comparison with the conventional PB equation, Eq. (8) incorporates an electric field-dependent local dielectric permittivity, ε_{eff}, which was proposed by Abrashkin *et al.*,[36] as well as Gongadze and Iglic earlier.[46]

Equating the electrochemical potentials for cations and anions in the EDL to those in the bulk solution yields

$$n_{\text{c}} = \frac{n\chi_{\text{c}}\exp\left(-\beta e_0\phi\right)}{\chi_{\text{c}}\gamma_{\text{c}}\exp\left(-\beta e_0\phi\right) + \chi_{\text{a}}\gamma_{\text{a}}\exp\left(\beta e_0\phi\right) + \left(1-\chi_{\text{c}}-\chi_{\text{a}}\right)\frac{\sinh\left(\mu_{\text{w}}^{\text{eff}}\beta|\nabla\phi|\right)}{\mu_{\text{w}}^{\text{eff}}\beta|\nabla\phi|}}, \tag{9}$$

$$n_{\text{a}} = \frac{n\chi_{\text{a}}\exp\left(\beta e_0\phi\right)}{\chi_{\text{c}}\gamma_{\text{c}}\exp\left(-\beta e_0\phi\right) + \chi_{\text{a}}\gamma_{\text{a}}\exp\left(\beta e_0\phi\right) + \left(1-\chi_{\text{c}}-\chi_{\text{a}}\right)\frac{\sinh\left(\mu_{\text{w}}^{\text{eff}}\beta|\nabla\phi|\right)}{\mu_{\text{w}}^{\text{eff}}\beta|\nabla\phi|}}, \tag{10}$$

where $\chi_{\text{c}} = n_{\text{c}}/n$ and $\chi_{\text{a}} = n_{\text{a}}/n$ are the bulk number density of cations and anions, respectively, normalized to n.

By substituting Eqs. (9) and (10) into Eq. (7), we obtain a single ordinary differential equation (ODE) that controls the electric potential distribution. The right boundary condition in the bulk solution is written as

$$\phi(x_{\text{bulk}}) = 0. \tag{11}$$

The OHP is defined as the left boundary, $x = 0$. Based on Eqs. (2)–(5), the left boundary condition is rearranged to

$$\phi(x=0) = \phi_{\text{M}} - \phi_{\text{S}} - \chi_{\text{M}} - \sigma_{\text{free}}\left(\frac{\delta_1}{\varepsilon_1} + \frac{\delta_2}{\varepsilon_2} + \frac{\delta_3}{\varepsilon_3}\right) - \frac{N_{\text{ad}}\theta_{\text{w}}\mu_{\text{w}}}{\varepsilon_2}\left[\coth\left(\frac{\mu_{\text{w}}E_{\text{loc}} + \delta\mu}{kT}\right) - \frac{kT}{\mu_{\text{w}}E_{\text{loc}} + \delta\mu}\right]. \tag{12}$$

According to the Gauss theorem, σ_{free} can be written as the gradient of ϕ, namely, $\sigma_{\text{free}} = -\varepsilon_{x=0}\left(\frac{\partial\phi}{\partial x}\right)_{x=0}$.[47] The applied electrode potential (E_{SHE}) can be written as $E_{\text{SHE}} = \phi_{\text{M}} - \phi_{\text{S}} - \mu_{\text{e}}^{\text{M}}/F - E_{\text{abs}}^{\text{SHE}}$, with F being the Faraday constant, $\mu_{\text{e}}^{\text{M}}$ being the chemical potential of the electrons in the metal electrode, and $E_{\text{abs}}^{\text{SHE}}$ being the absolute potential of the standard hydrogen electrode (SHE). Equation (12) is reformulated as

$$\phi(x=0) = E_{\text{SHE}} - E_{\text{pzfc,SHE}}^{0} + \varepsilon_{x=0}\left(\frac{\partial\phi}{\partial x}\right)_{x=0}\left(\frac{\delta_1}{\varepsilon_1} + \frac{\delta_2}{\varepsilon_2} + \frac{\delta_3}{\varepsilon_3}\right) - \frac{N_{\text{ad}}\theta_{\text{w}}\mu_{\text{w}}}{\varepsilon_2}\left[\coth\left(\frac{\mu_{\text{w}}E_{\text{loc}} + \delta\mu}{kT}\right) - \frac{kT}{\mu_{\text{w}}E_{\text{loc}} + \delta\mu}\right], \tag{13}$$

where $E_{\text{pzfc,SHE}}^{0} = \chi_{\text{M}} - \mu_{\text{e}}^{\text{M}}/F - E_{\text{abs}}^{\text{SHE}}$. $E_{\text{pzfc,SHE}}^{0}$ already accounts for the pzfc shift due to the electronic polarization of the adsorbed water molecules.

D. Double-layer capacitance

The differential double-layer capacitance, C_{dl}, is defined as

$$\frac{1}{C_{\text{dl}}} = \frac{\partial E_{\text{SHE}}}{\partial\sigma_{\text{free}}}. \tag{14}$$

Based on the definition of Eq. (15), by taking the partial derivative of both sides of Eq. (13) with respect to σ_{free}, we obtain

$$\frac{1}{C_{\text{dl}}} = \frac{1}{C_{\text{str}}} + \frac{1}{C_{\text{dl,dif}}} + \frac{1}{C_{\text{w}}}. \tag{15}$$

Here C_{str}, $C_{\text{dl,dif}}$, and C_{w} are capacitances of the EDL structure, the diffuse layer, and water dipole layer, written as, respectively,

$$\frac{1}{C_{\text{str}}} = \frac{\delta_1}{\varepsilon_1} + \frac{\delta_2}{\varepsilon_2} + \frac{\delta_3}{\varepsilon_3}, \tag{16}$$

$$\frac{1}{C_{\text{dl,dif}}} = \frac{\partial\Delta\phi_{\text{OHP}}^{\text{S}}}{\partial\sigma_{\text{free}}}, \tag{17}$$

$$\frac{1}{C_{\text{w}}} = \frac{\partial\Delta\phi_{\text{w}}}{\partial\sigma_{\text{free}}} = \frac{N_{\text{ad}}\theta_{\text{w}}\mu_{\text{w}}^2}{kT\varepsilon_2^2} \times\left\{\frac{1}{\sinh^2[(-\mu_{\text{w}}\sigma_{\text{free}}/\varepsilon_2 + \delta\mu)/kT]} - \frac{1}{[(-\mu_{\text{w}}\sigma_{\text{free}}/\varepsilon_2 + \delta\mu)/kT]^2}\right\}. \tag{18}$$

E. Model parameterization

This model comprises five sets of parameters, as listed in Table I, termed "constant," "electrolyte solution properties," "EDL structure," "adsorbed water molecules," and "metal electrode." The following analysis focuses on sensitive model parameters, according to a parametric sensitivity analysis provided in the supplementary material.

The parameters of the electrolyte solution correspond to 1 mM $HClO_4$[23] and 1 mM $HClO_4$ + 8 mM $XClO_4$(X = Li^+, Na^+, K^+).[28] Hydrated diameters of ions are cited from Nightingale's work.[30] d_{H^+}, d_{Li^+}, d_{Na^+}, d_{K^+}, and $d_{ClO_4^-}$ are 5.6, 7.6, 7.16, 6.6, and 6.76 Å, respectively. By utilizing the formula for the effective dielectric permittivity provided in Eq. (8), we derive the bulk dielectric permittivity, represented as $\varepsilon_{\text{b}} = \varepsilon_{\infty} + (\mu_{\text{w}}^{\text{eff}})^2 n_{\text{s}}^{\text{b}}/(3kT)$. Consequently, we determine the effective dipole moment of water molecules to be $\mu_{\text{w}}^{\text{eff}} = \sqrt{3kT(\varepsilon_{\text{b}} - \varepsilon_{\infty})/n_{\text{s}}^{\text{b}}}$.

The parameters of the EDL structure include ε_i and δ_i (i = 1, 2, 3). When an electron tail exists in the gap layer, ε_1 should exceed the vacuum permittivity ε_0. Herein, we set $\varepsilon_1 = 10\varepsilon_0$ to encompass the influence of electrons escaping from Au(111).[18] Li *et al.* gave a gap layer thickness of ~1.5Å at Au(111) using AIMD simulations. Therefore, we use δ_1 = 1.5Å. Li *et al.* and Xu *et al.* calculated that the distance between the nearest layer of water and Au(111) is 3 ~ 4Å.[48,49] We use an average value in this range, 3.5Å. Therefore, the thickness of the gap between the CAP and the ASP, δ_2, is about 2Å. Parsons determined that ε_2 is 7.5 ε_0.[50] Bockris suggested that ε_3 is 30ε_0.[51] The values of ε_2 = 7.5 ε_0 and ε_3 = 35 ε_0, used in this work, are closed to those used by Parsons and Bockris. For the space between the ASP and OHP, we adopt δ_3 = 3Å, a representative radius for hydrated ions.

The parameters of the adsorbed water molecules in the first layer contain θ_{w}, μ_{w}, and δu. Le and Cheng calculated a total coverage of ~0.5 and ~0.55, for adsorbed water molecules at Pt(111) and Ag(111), respectively.[13,15] In our model, the adsorbed water coverage refers to the total coverage of all chemisorbed and physiosorbed

TABLE I. Model parameters of the base case.

Symbol	Value	Physical significance
	Constants	
k(J/K)	1.38×10^{-23}	Boltzmann constant
e_0(C)	1.6×10^{-19}	Elementary charge
N_A(/mol)	6.02×10^{-23}	Avogadro constant
F(C/mol)	96 485	Faraday constant
h(J/s)	6.626×10^{-34}	Planck constant
ε_0(F/m)	8.85×10^{-11}	Vacuum permittivity
ε_b(F/m)	78.5 ε_0	Permittivity of bulk water
T(K)	298	Temperature
	Electrolyte solution properties	
d_s(Å)	2.75[45]	Diameter of water molecules
d_{H^+}(Å)	5.6[30]	Effective diameter of solvated H^+
d_{Li^+}(Å)	7.6[30]	Effective diameter of solvated Li^+
d_{Na^+}(Å)	7.16[30]	Effective diameter of solvated Na^+
d_{K^+}(Å)	6.6[30]	Effective diameter of solvated K^+
$d_{ClO_4^-}$(Å)	6.76[30]	Effective diameter of solvated ClO_4^-
n_s^b(/m^3)	55 600	Bulk number density of water
$n_{H^+}^b$(/m^3)	$1N_A$	Bulk number density of H^+
n_{Li^+,Na^+,K^+}^b(/m^3)	8 N_A	Bulk number density of Li^+, Na^+, K^+
$n_{ClO_4^-}^b$(/m^3)	$[1,9]N_A$	Bulk number density of ClO_4^-
ε_∞(F/m)	1.8 ε_0	Optical permittivity
μ_w^{eff}(C m)	$\sqrt{3kT(\varepsilon_b - \varepsilon_\infty)/n_s^b}$	Effective dipole moment of water molecules
	EDL structure	
ε_1(F/m)	10 ε_0[18]	Permittivity between the electrode and the CAP
ε_2(F/m)	7.5 ε_0[50]	Permittivity between the CAP and the ASP
ε_3(F/m)	35 ε_0[51]	Permittivity between the ASP and the OHP
δ_1(Å)	1.5[48]	Thickness between the electrode and the CAP
δ_2(Å)	2[48,49]	Thickness between the CAP and the ASP
δ_3(Å)	3[18]	Thickness between the ASP and the OHP
	Adsorbed water molecules	
θ_w	0.55[13,15]	Coverage of adsorbed water molecules
μ_w(C m)	$1.85 \times 3.335 \times 10^{-35}$	Intrinsic dipole moment of water molecule
$\delta u(kT)$	1[48,49,53]	Au(111)-water interaction
	Metal electrode	
$a_{Au(111)}$(Å)	4.08	Lattice constant of the Au(111) electrode
N_{ad}(/m^2)	1.39×10^{19}	Calculated using $4/(\sqrt{3}a_{Au111}^2)$
$E_{pzfc,SHE}^0$(V)	0.30	pzfc when $\delta u = 0$

water molecules at the interface. Density functional theory (DFT) calculations of Melander *et al.* showed similar coverage of the water layer for Pt, Au, and Ag,[52] so we used a value of 0.55 for Au(111). As for μ_w, we adopt the intrinsic dipole moment of a water molecule, μ_w = 1.85 D. Groβ and Sakong employed an ice-like water bilayer model to compute the adsorption energy of O-down and H-down water configurations on various metals. The O-down and H-down orientations correspond to α_w values of 0 and π in this work, respectively. According to their calculations, the adsorption energies of O-down and H-down water at Au(111) are −0.41 and −0.43 eV, respectively.[53] Therefore, we use $\delta u \approx 1$ kT at the Au(111), indicating that the H atoms of the first-layer water molecules are closer to

the uncharged Au(111) than the O atoms. Recently, Xu *et al.* calculated the distribution of water molecules at the Au(111) using three functionals: BEEF-vdW, RPBE-D3, and PBE-D3 through AIMD.[49] A distinct H peak appeared at about 2Å from the Au(111), while the O peak appeared at around 3Å, slightly farther than the H peak, due to its hydrophobicity.[54]

Considering the Au(111) as the metal, we have $N_{ad} = 1.39 \times 10^{19}/m^2$ base on a lattice constant of 4.08Å. The pzfc of the Au(111) in the 0.01M $HClO_4$ solution is $E_{pzfc,SHE} = 0.53\ V_{SHE}$.[55] Considering that the orientational polarization of chemisorbed water increases the pzfc by 0.23 V, $E^0_{pzfc,SHE}$, excluding this dipole effect, would be $0.30\ V_{SHE}$.

III. RESULTS AND DISCUSSION

A. Origins of peaks in C_{dl} at Au(111)-aqueous solution interfaces

The C_{dl} profile based on the full model is denoted as curve I in Fig. 2(b) for the Au(111) in 1 mM $HClO_4$ solution at 298 K. The full model [Case I in Fig. 2(a)] comprehensively accounts for the orientational polarization effect of first-layer water molecules, chemical interactions between water molecules and the Au(111), the asymmetric steric effect of ions, and the electric field-dependent dielectric permittivity. Previously, Schwarz and Sundararaman employed the Nonlinear Electrochemical Soft-Sphere (NESS) solvation model to capture the capacitance features observed experimentally at the Ag(100)–KPF_6 solution interface.[33,34] As an extension to the NESS model, our model further incorporates the adsorption energy difference ($\delta\mu$) between H-down and O-down water configurations. This comprehensive model allows for a detailed analysis of different factors influencing the peaks observed in the capacitance curves.

The full model's results align closely with the experimental data obtained for C_{dl} of the Au(111) in the 1 mM $HClO_4$ solution.[23] The much higher anodic peak of C_{dl} compared to the cathodic peak is observed. This disparity arises primarily due to a net preferential orientation of water molecules with H-down at an uncharged Au(111) surface. Consequently, these H-down water molecules have a greater capacity to screen positive σ_{free}, which intends to rotate water molecules toward the O-down configuration ($\alpha_w = 0$); see the Curve I in Fig. 2(c). Hence, the anodic peak of C_{dl} is much higher than the cathodic peak. At 0.3 V_{SHE} corresponding to the cathodic peak, the concentration of $c^{OHP}_{H^+}$ is ~0.31M, far below its

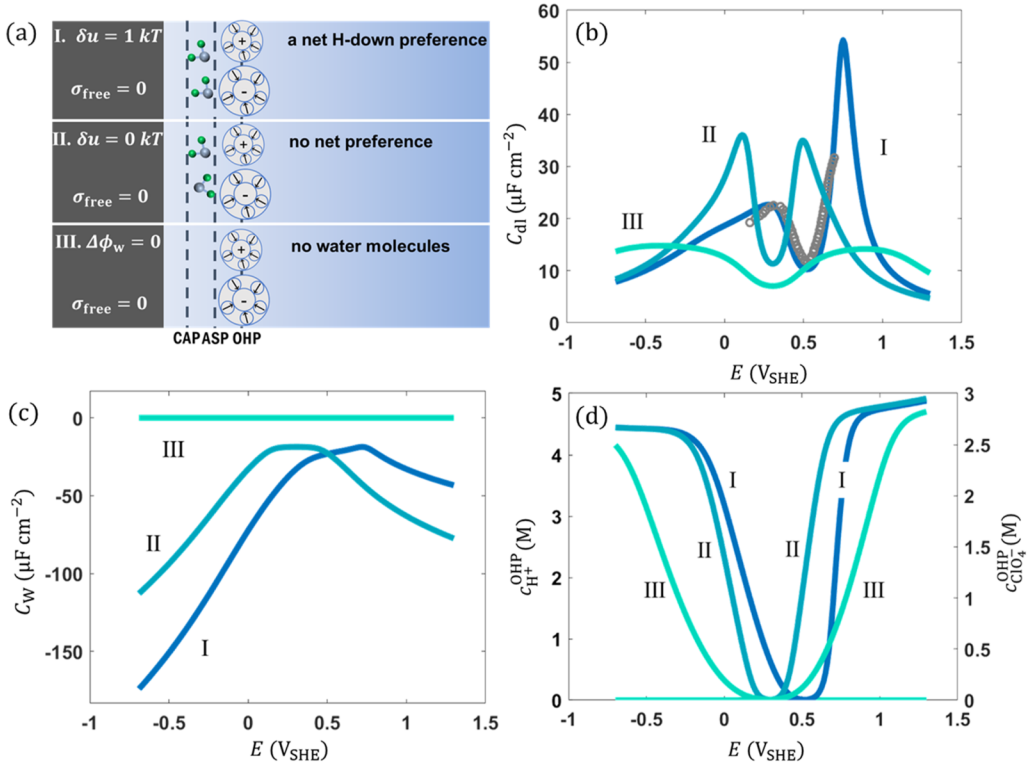

FIG. 2. (a) Schematic diagrams of three different models of the inner layer of the EDL. Case I is the full model. In the full model, ε_{eff} and $\langle\cos\alpha_w\rangle$ are field-dependent expressed in Eqs. (5) and (8), respectively, with $\delta\mu = 1$ kT. Keeping other physical quantities unchanged and letting $\delta\mu = 0$ kT, we can get case II. By further letting $\Delta\phi_w = 0$ [Eq. (4)], we obtain case III. (b) C_{dl} as a function of electrode potential for the three cases. The electrolyte concentration is 1 mM $HClO_4$. The experimental data, shown in circles, are taken from Hamelin's work.[23] (c) Capacitance associated with the orientational polarization of the first-layer water molecules, C_W, as a function of electrode potential, calculated by Eq. (18). (d) The concentrations of hydrated protons $c^{OHP}_{H^+}$ and hydrated perchlorate ions $c^{OHP}_{ClO_4^-}$ on the OHP as a function of the electrode potential.

saturation concentration (~4.5M), meaning that ion overcrowding does not occur yet at the cathodic peak.

We have also considered the effect of partial desolvation of counterions on the peak of the double-layer capacitance.[56] The resulting influence on C_{dl} is mainly limited to the two tails of the capacitance curve, as shown in Fig. S3 in the supplementary material, while the location and height of two capacitance peaks are largely unchanged.

Setting the full model as a baseline, curve II is derived by ignoring the metal–water interaction, setting $\delta\mu = 0$ kT [Case II in Fig. 2(a)]. Compared to curve I, two notable differences are observed for the curve II. On the one hand, the pzfc shifts negative at $\delta\mu = 0$ kT. When $\delta\mu > 0$, the water molecules in the first layer tend to adopt the $\alpha_w = \pi$ (H-down) orientation. This configuration leads to an extra potential decrease and a more positive $E_{pzfc,SHE}$. On the other hand, a higher cathodic peak of C_{dl} is observed in the case II that ignores the metal–water interaction. The growth in the cathodic peak reflects the smaller diameter of hydrated H^+ ions compared to hydrated ClO_4^- ions,[26] which results in a greater concentration for $c_{H^+}^{OHP}$ (~1.1M at 0.1 V_{SHE}) than that for $c_{ClO_4^-}^{OHP}$ (~0.9M at 0.5 V_{SHE}). However, neither of them reaches their overcrowding concentrations, as shown in Fig. 2(d).

Furthermore, by ignoring the influence of the electric potential drop caused by water molecules, $\Delta\phi_w$ [case III in Fig. 2(a)], we obtain curve III. Compared to the case II, the position of the pzfc remains unchanged, and there is no alteration in the relative heights of the double peaks. Nevertheless, a noticeable broadening of both peaks occurs, and the shape of the C_{dl} curve diverges significantly from the experimental curve. Comparing curve II and curve III in Fig. 2(b), we find that the negative capacitance component contributed by water molecules [curves I and II in Fig. 2(c)] increases the overall C_{dl}. The negative capacitance results primarily from the shielding effect of interfacial water molecules, inducing a potential drop in a direction opposite that caused by the free excess charge on the metal surface. This means a negative capacitance, according to Eq. (18) $\left(\frac{1}{C_w} = \frac{\partial\Delta\phi_w}{\partial\sigma_{free}}\right)$.

The above-mentioned findings suggest that the orientational polarization of water molecules in the first layer and the metal–water interactions significantly raise the anodic peak of C_{dl} compared to the cathodic peak, indicating that the relative heights of the two peaks cannot be solely determined based on the size of hydrated cations and anions. Moreover, at the Au(111)–aqueous solution interface, the origins of capacitance peaks are caused by saturated orientational polarization of interfacial water molecules, rather than

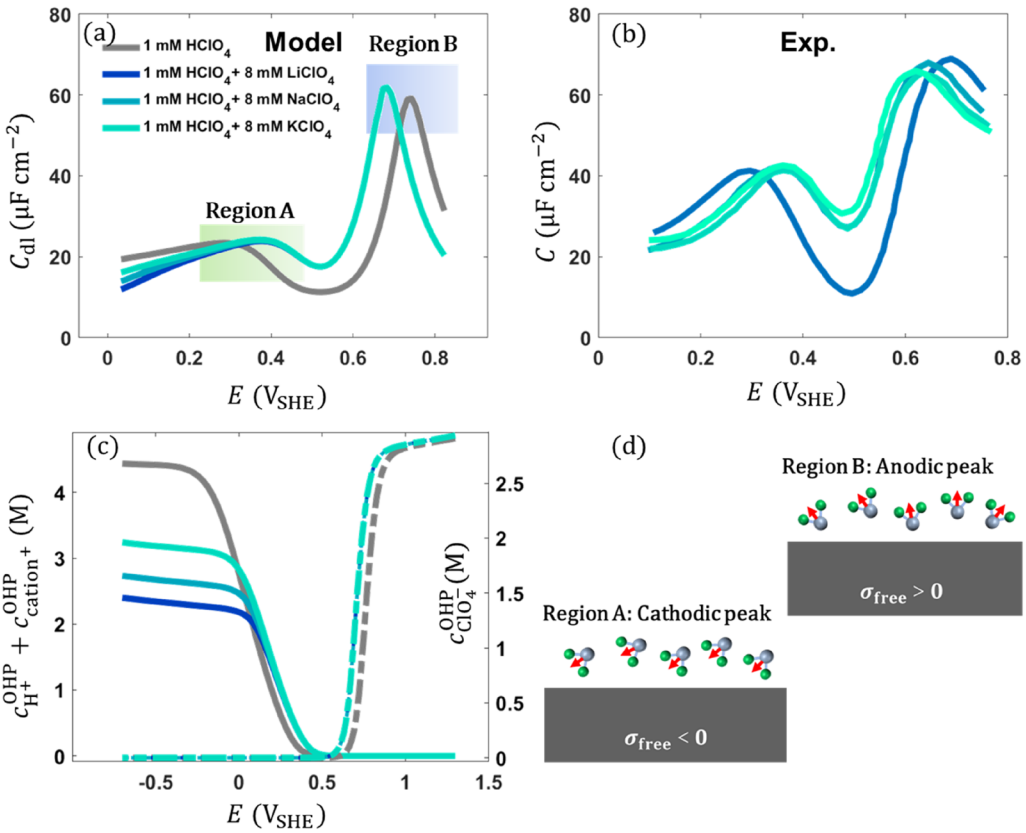

FIG. 3. C_{dl} curves at the Au(111)-aqueous solution interfaces as a function of the electrode potential in different electrolyte solutions. (a) Shows the model's results, and (b) shows experimental data, taken from the Ref. 28. (c) The total concentrations of hydrated cations (solid line) and hydrated perchlorate (dash-dot line) at the OHP. (d) Schematic diagram of the orientation of the first-layer water molecules corresponding to the cathodic peak and anodic peak, respectively.

overcrowding counterions. To further corroborate this view, we examine the cation dependence of the C_{dl} peaks.

B. Cation dependence of C_{dl} at Au(111)-aqueous solution interfaces

Figure 3(a) shows that cation-dependent C_{dl} profiles at the Au(111)–aqueous solution interfaces calculated using the model. Model-based and experimental data are plotted in the same graph in Fig. S4 for a direct comparison. All the parameters used here are the same as in Fig. 3. Hydrated diameters of ions are directly cited from Nightingale's work.[30] d_{H^+}, d_{Li^+}, d_{Na^+}, d_{K^+}, and $d_{ClO_4^-}$ are 5.6, 7.6, 7.16, 6.6, and 6.76 Å, respectively. The model results are consistent with the experimental results: the cathodic peaks of the C_{dl} curves hardly change with the size of the hydrated cations. At 0.38 V_{SHE}, corresponding to the cathodic peak of the C_{dl} curves, the total concentration of hydrated cations at the OHP are all at around 0.27M [Fig. 3(c)], which is far below their respective overcrowding concentrations.

Cation dependence of C_{dl} further corroborates the view that the peaks are not caused by overcrowding of hydrated ions. Our analysis supports the view of Schwarz and Sundararaman[34] that two peaks of the camel-shaped C_{dl} curves are caused by the nonlinear dielectric response of interfacial water molecules in dilute electrolyte solutions. While the ion crowding effect can generate a camel-shaped C_{dl} profile, its simulated magnitude remains significantly lower than experimental values [Curve III in Fig. 2(b)]. This effect dominates in solvent-free ionic liquids.[26] However, nonadsorbing aqueous electrolytes exhibit dielectric saturation as the primary driver of capacitance peaks, owing to its high dielectric permittivity and the proximity of water molecules to the electrode surface.[33,34]

Figure 3(d) shows the schematic diagram of the orientation of the first-layer water molecules in the ASP corresponding to the cathodic peak and anodic peak in Fig. 3(a), respectively. When σ_{free} is negative, the water molecules in ASP adopt an O-down configuration to shield the electric field; following the line of reasoning, when σ_{free} is positive, they adopt a H-down configuration to shield the electric field. Moreover, the orientation of water molecules depends only on the free charge of the surface and is not an explicit function of the type of cation in the solution. Therefore, both peaks of C_{dl} curves are caused mainly by the saturation of the orientational polarization of interfacial water molecules. The overcrowding effect of hydrated ions is reflected in the tail of the C_{dl} curves. The higher the concentration of cations at the OHP, the higher the tail. As for the difference of the anodic peak of the C_{dl} curves in the experiment, it may be due to the weak adsorption of ClO_4^- and/or potential-dependent reconstruction.[28,57]

C. Temperature effects of C_{dl} at Au(111)-aqueous solution interfaces

The orientational polarization effect of first-layer water molecules and the metal–water interactions play a crucial role in shaping the peaks of C_{dl} at Au(111), as revealed in the proceeding discussion. The temperature dependence of C_{dl} constitutes an additional test of this mechanism.

Figures 4(a) and 4(b) shows the model–experiment comparison of C_{dl} curves for Au(111) in 1 mM $HClO_4$ solution at different temperatures.[23] Model-based and experimental data are plotted in the same graph in Fig. S5. The simulated C_{dl} curves align well with the experimental capacitance data. The model parameters except dielectric permittivities ($\varepsilon_1, \varepsilon_2, \varepsilon_3, \varepsilon_{bulk}$) are fixed at their base values. Temperature-dependent dielectric permittivities are listed in Table II. Following the temperature dependence of dielectric permittivity of bulk water,[58] the interfacial dielectric permittivities, $\varepsilon_1, \varepsilon_2$, and ε_3 also decrease with increasing temperature. The model captures the positive shift in the pzfc as temperature increases; it can be understood by Eq. (13). At the pzfc, based on the definition, $\sigma_{free} = 0$, Eq. (13) is simplified to

$$E_{pzfc,SHE} - E^0_{pzfc,SHE} = \frac{N_{ad}\theta_w\mu_w}{\varepsilon_2}\left[\coth\left(\frac{\delta\mu}{kT}\right) - \frac{kT}{\delta\mu}\right]. \quad (19)$$

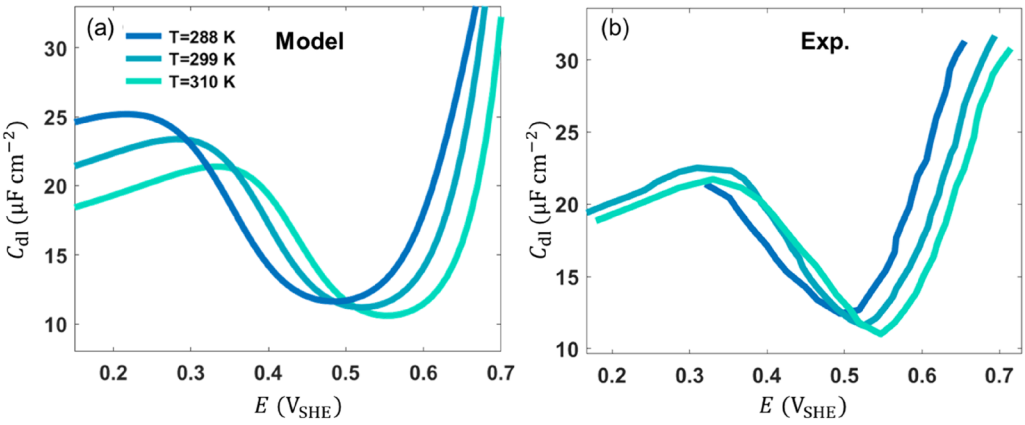

FIG. 4. C_{dl} curves at Au(111)-aqueous solution interfaces as a function of the electrode potential in 1 mM $HClO_4$ solution at different temperatures. (a) Shows the model results, and (b) shows experimental data, taken from the Ref. 23.

TABLE II. Temperature-dependent dielectric permittivities.

	ε_1	ε_2	ε_3	ε_{bulk}[58]
288 K	$12\varepsilon_0$	$9.0\varepsilon_0$	$38.5\varepsilon_0$	$82.04\varepsilon_0$
299 K	$10\varepsilon_0$	$7.5\varepsilon_0$	$35\varepsilon_0$	$78.52\varepsilon_0$
310 K	$8\varepsilon_0$	$6.5\varepsilon_0$	$31.5\varepsilon_0$	$74.85\varepsilon_0$

In Eq. (19), the term on the right-hand side represents the pzfc shift caused by the orientational polarization of adsorbed water molecules, which is induced by the metal–water interaction in the absence of an external electric field. Because of $\delta\mu = 1\ \mathrm{kT} > 0$, values of the term on the right are greater than 0. The smaller the parameter ε_2, the bigger the term $E_{\mathrm{pzfc,SHE}} - E^0_{\mathrm{pzfc,SHE}}$. This means that there is a greater potential drop due to the orientational polarization of adsorbed water molecules. Therefore, as the temperature increases, ε_2 decreases and pzfc moves to a higher potential. Moreover, both the model and experiments show that the cathodic peaks decrease with increasing temperature, because a higher temperature reduces the dielectric permittivity, thus diminishing the interfacial water molecules' ability to shield the interfacial electric field and lowering the charge storage capacity.

IV. CONCLUSION

This study offers new insights into the origins of double-layer capacitance peaks at the Au(111)–aqueous solution interface, challenging the prevailing view that these peaks are solely due to counterion overcrowding. Our analysis is based on a refined model for the EDL that accounts for the orientational polarization of interfacial water molecules, asymmetric ion steric effects, and a field-dependent dielectric permittivity. The model reveals that the relative heights of the anodic and cathodic peaks are influenced by the orientational polarization of water molecules. The model's agreement with experimental data and its ability to capture the cation dependence of capacitance peaks further validate the new perspective of capacitance peaks. The temperature dependency of the capacitance profile is also explained by the effect of temperature on the dielectric permittivities and the orientational polarization of interfacial water. This work provides a deeper understanding of the processes governing EDL structure and capacitive behavior, emphasizing the pivotal role of interfacial water molecules.

SUPPLEMENTARY MATERIAL

See the supplementary material for the following: statistical model of the first-layer water, parameter sensitivity analysis of the electric double layer (EDL) structure and adsorbed water molecules, detailed analysis of the impact of partial desolvation on double-layer capacitance, model–experiment comparison for cation dependence of double-layer capacitance, and model–experiment comparison for temperature dependence of double-layer capacitance.

ACKNOWLEDGMENTS

This work was supported by the National Natural Science Foundation of China (Grant No. 22172151). J.H. is supported by the Initiative and Networking Fund of the Helmholtz Association (Grant No. VH-NG-1709) and the European Research Council (ERC) Starting Grant (MESO-CAT, Grant Agreement No. 101163405).

AUTHOR DECLARATIONS

Conflict of Interest

The authors have no conflicts to disclose.

Author Contributions

Erfei Zhen: Conceptualization (equal); Data curation (equal); Formal analysis (equal); Methodology (equal); Software (equal); Validation (equal); Visualization (equal); Writing – original draft (equal); Writing – review & editing (equal). **Yanxia Chen**: Conceptualization (equal); Funding acquisition (equal); Validation (equal). **Jun Huang**: Conceptualization (equal); Data curation (equal); Formal analysis (equal); Methodology (equal); Validation (equal); Writing – original draft (equal); Writing – review & editing (equal).

DATA AVAILABILITY

The data that support the findings of this study are available within the article and its supplementary material.

REFERENCES

[1] J. O. M. Bockris, B. E. Conway, E. Yeager, and R. E. White, *Comprehensive Treatise of Electrochemistry* (Springer, 1980).
[2] W. Schmickler and E. Santos, *Interfacial Electrochemistry* (Springer Science & Business Media, 2010).
[3] P. W. Atkins, J. De Paula, and J. Keeler, *Atkins' Physical Chemistry* (Oxford University Press, 2023).
[4] W. Stumm, *Chemistry of the Solid-Water Interface* (Wiley, New York, 1992).
[5] W. R. Fawcett, "Fifty years of studies of double layer effects in electrode kinetics—A personal view," J. Solid State Electrochem. **15**, 1347–1358 (2011).
[6] L. Blum, "Structure of the electric double layer," Adv. Chem. Phys. **78**, 171–222 (1990).
[7] C. Merlet, B. Rotenberg, P. A. Madden, P.-L. Taberna, P. Simon, Y. Gogotsi, and M. Salanne, "On the molecular origin of supercapacitance in nanoporous carbon electrodes," Nat. Mater. **11**(4), 306–310 (2012).
[8] M. Salanne, B. Rotenberg, K. Naoi, K. Kaneko, P. L. Taberna, C. P. Grey, B. Dunn, and P. Simon, "Efficient storage mechanisms for building better supercapacitors," Nat. Energy **1**(6), 16070 (2016).
[9] J. Wu, "Understanding the electric double-layer structure, capacitance, and charging dynamics," Chem. Rev. **122**(12), 10821–10859 (2022).
[10] R. Guidelli and W. Schmickler, "Recent developments in models for the interface between a metal and an aqueous solution," Electrochim. Acta **45**(15–16), 2317–2338 (2000).
[11] D. C. Grahame, "The electrical double layer and the theory of electrocapillarity," Chem. Rev. **41**(3), 441–501 (1947).
[12] R. Parsons, "The electrical double layer: Recent experimental and theoretical developments," Chem. Rev. **90**(5), 813–826 (1990).
[13] J.-B. Le, Q.-Y. Fan, J.-Q. Li, and J. Cheng, "Molecular origin of negative component of Helmholtz capacitance at electrified Pt(111)/water interface," Sci. Adv. **6**(41), eabb1219 (2020).

[14]X. Wang, Y. Wang, Y. Kuang, and J.-B. Le, "Understanding the effects of electrode material, single crystal facet, and electrolyte ion on the Helmholtz capacitance of metal/aqueous solution interfaces," J. Phys. Chem. Lett. **14**(35), 7833–7839 (2023).
[15]L. Li, Y.-P. Liu, J.-B. Le, and J. Cheng, "Unraveling molecular structures and ion effects of electric double layers at metal water interfaces," Cell Rep. Phys. Sci. **3**(2), 100759 (2022).
[16]J.-B. Le and J. Cheng, "Modeling electrified metal/water interfaces from ab initio molecular dynamics: Structure and Helmholtz capacitance," Curr. Opin. Electrochem. **27**, 100693 (2021).
[17]J.-B. Le, A. Chen, L. Li, J.-F. Xiong, J. Lan, Y.-P. Liu, M. Iannuzzi, and J. Cheng, "Modeling electrified Pt(111)-H_{ad}/water interfaces from ab initio molecular dynamics," JACS Au **1**(5), 569–577 (2021).
[18]J. Huang, "Zooming into the inner Helmholtz plane of Pt(111)–aqueous solution interfaces: Chemisorbed water and partially charged ions," JACS Au **3**(2), 550–564 (2023).
[19]G. Valette, "Double layer on silver single-crystal electrodes in contact with electrolytes having anions which present a slight specific adsorption: Part I. The (110) face," J. Electroanal. Chem. Interfacial Electrochem. **122**, 285–297 (1981).
[20]G. Valette, "Double layer on silver single crystal electrodes in contact with electrolytes having anions which are slightly specifically adsorbed: Part II. The (100) face," J. Electroanal. Chem. Interfacial Electrochem. **138**(1), 37–54 (1982).
[21]A. Hamelin, M. L. Foresti, and R. Guidelli, "Test of the Gouy-Chapman theory at a (111) silver single-crystal electrode," J. Electroanal. Chem. **346**(1–2), 251–259 (1993).
[22]A. Hamelin and L. Stoicoviciu, "Study of gold low index faces in KPF_6 solutions: Part I. Experimental behaviour and determination of the points of zero charge," J. Electroanal. Chem. Interfacial Electrochem. **234**(1–2), 93–105 (1987).
[23]F. Silva, M. J. Sottomayor, and A. Hamelin, "The temperature coefficient of the potential of zero charge of the gold single-crystal electrode/aqueous solution interface: Possible relevance to gold-water interactions," J. Electroanal. Chem. Interfacial Electrochem. **294**(1–2), 239–251 (1990).
[24]K. Ojha, K. Doblhoff-Dier, and M. T. M. Koper, "Double-layer structure of the Pt(111)–aqueous electrolyte interface," Proc. Natl. Acad. Sci. U. S. A. **119**(3), e2116016119 (2022).
[25]L.-L. Zhang, C.-K. Li, and J. Huang, "A beginners' guide to modelling of electric double layer under equilibrium, nonequilibrium and AC conditions," J. Electrochem. **28**(2), 2108471 (2022).
[26]A. A. Kornyshev, "Double-layer in ionic liquids: paradigm change?," J. Phys. Chem. B **111**, 5545–5557 (2007).
[27]F. Nattino, M. Truscott, N. Marzari, and O. Andreussi, "Continuum models of the electrochemical diffuse layer in electronic-structure calculations," J. Chem. Phys. **150**(4), 041722 (2018).
[28]A. Adnan, S. Behjati, N. Félez-Guerrero, K. Ojha, and M. T. M. Koper, "Tracking the surface structure and the influence of cations and anions on the double-layer region of a Au(111) electrode," Phys. Chem. Chem. Phys. **26**, 21419 (2024).
[29]K. Ojha, N. Arulmozhi, D. Aranzales, and M. T. M. Koper, "Double layer at the Pt(111)–aqueous electrolyte interface: Potential of zero charge and anomalous Gouy–Chapman screening," Angew. Chem. **132**(2), 721–725 (2020).
[30]E. R. Nightingale, Jr., "Phenomenological theory of ion solvation. Effective radii of hydrated ions," J. Phys. Chem. **63**(9), 1381–1387 (1959).
[31]G. Valette, "Double layer on silver single crystal electrodes in contact with electrolytes having anions which are slightly specifically adsorbed: Part III. The (111) face," J. Electroanal. Chem. Interfacial Electrochem. **269**(1), 191–203 (1989).
[32]J. Huang, "Density-potential functional theory of electrochemical double layers: Calibration on the Ag(111)-KPF_6 system and parametric analysis," J. Chem. Theory Comput. **19**(3), 1003–1013 (2023).
[33]R. Sundararaman, K. Letchworth-Weaver, and K. A. Schwarz, "Improving accuracy of electrochemical capacitance and solvation energetics in first-principles calculations," J. Chem. Phys. **148**(14), 144105 (2018).
[34]K. Schwarz and R. Sundararaman, "The electrochemical interface in first-principles calculations," Surf. Sci. Rep. **75**(2), 100492 (2020).
[35]F. Booth, "The dielectric constant of water and the saturation effect," J. Chem. Phys. **19**(4), 391–394 (1951).
[36]A. Abrashkin, D. Andelman, and H. Orland, "Dipolar Poisson-Boltzmann equation: Ions and dipoles close to charge interfaces," Phys. Rev. Lett. **99**(7), 077801 (2007).
[37]D. Gunceler, K. Letchworth-Weaver, R. Sundararaman, K. A. Schwarz, and T. A. Arias, "The importance of nonlinear fluid response in joint density-functional theory studies of battery systems," Modell. Simul. Mater. Sci. Eng. **21**(7), 074005 (2013).
[38]A. Groß and S. Sakong, "Ab initio simulations of water/metal interfaces," Chem. Rev. **122**(12), 10746–10776 (2022).
[39]L. Braunwarth, C. Jung, and T. Jacob, "Potential-dependent Pt(111)/water interface: Tackling the challenge of a consistent treatment of electrochemical interfaces," ChemPhysChem **24**(1), e202200336 (2023).
[40]J. Huang, "Surface charging behaviors of electrocatalytic interfaces with partially charged chemisorbates," Curr. Opin. Electrochem. **33**, 100938 (2022).
[41]G. Kastlunger, P. Lindgren, and A. A. Peterson, "Controlled-potential simulation of elementary electrochemical reactions: Proton discharge on metal surfaces," J. Phys. Chem. C **122**(24), 12771–12781 (2018).
[42]J. Huang, A. Malek, J. Zhang, and M. H. Eikerling, "Non-monotonic surface charging behavior of platinum: A paradigm change," J. Phys. Chem. C **120**(25), 13587–13595 (2016).
[43]J. Huang, T. Zhou, J. Zhang, and M. Eikerling, "Double layer of platinum electrodes: Non-monotonic surface charging phenomena and negative double layer capacitance," J. Chem. Phys. **148**(4), 044704 (2018).
[44]J. Huang, S. Chen, and M. Eikerling, "Grand-canonical model of electrochemical double layers from a hybrid density–potential functional," J. Chem. Theory Comput. **17**(4), 2417–2430 (2021).
[45]J. Huang, M. Li, M. J. Eslamibidgoli, M. Eikerling, and A. Groß, "Cation overcrowding effect on the oxygen evolution reaction," JACS Au **1**(10), 1752–1765 (2021).
[46]E. Gongadze and A. Iglič, "Decrease of permittivity of an electrolyte solution near a charged surface due to saturation and excluded volume effects," Bioelectrochemistry **87**, 199–203 (2012).
[47]A. J. Bard, L. R. Faulkner, and H. S. White, *Electrochemical Methods: Fundamentals and Applications* (John Wiley & Sons, 2022).
[48]C.-Y. Li, J.-B. Le, Y.-H. Wang, S. Chen, Z.-L. Yang, J.-F. Li, J. Cheng, and Z.-Q. Tian, "In situ probing electrified interfacial water structures at atomically flat surfaces," Nat. Mater. **18**(7), 697–701 (2019).
[49]M. Xu, S. Liu, S. Vijay, T. Bligaard, and G. Kastlunger, "Benchmarking water adsorption on metal surfaces with *ab initio* molecular dynamics," J. Chem. Phys. **160**(24), 244707 (2024).
[50]R. Parsons, "The structure of the mercury-electrolyte interphase in the presence of thiourea," Proc. R. Soc. London, Ser. A **261**(1304), 79–90 (1961).
[51]J. M. Bockris, M. Devanathan, and K. Müller, "On the structure of charged interfaces," in *Electrochemistry* (Elsevier, 1965), pp. 832–863.
[52]F. Domínguez-Flores, T. Kiljunen, A. Groß, S. Sakong, and M. M. Melander, "Metal–water interface formation: Thermodynamics from *ab initio* molecular dynamics simulations," J. Chem. Phys. **161**(4), 044705 (2024).
[53]S. Schnur and A. Groß, "Properties of metal–water interfaces studied from first principles," New J. Phys. **11**(12), 125003 (2009).
[54]V. Wieser, P. Bilotto, U. Ramach, H. Yuan, K. Schwenzfeier, H.-W. Cheng, and M. Valtiner, "Novel *in situ* sensing surface forces apparatus for measuring gold versus gold, hydrophobic, and biophysical interactions," J. Vac. Sci. Technol. A **39**(2), 023201 (2021).
[55]S. Trasatti and E. Lust, "The potential of zero charge," in *Modern Aspects of Electrochemistry* (Springer, 1999), pp. 1–215.
[56]S. R. Alfarano, S. Pezzotti, C. J. Stein, Z. Lin, F. Sebastiani, S. Funke, C. Hoberg, I. Kolling, C. Y. Ma, K. Mauelshagen *et al.*, "Stripping away ion hydration shells in electrical double-layer formation: Water networks matter," Proc. Natl. Acad. Sci. U. S. A. **118**(47), e2108568118 (2021).
[57]L. A. Kibler, J. M. Hermann, A. Abdelrahman, A. A. El-Aziz, and T. Jacob, "New insights on hydrogen evolution at Au single crystal electrodes," Curr. Opin. Electrochem. **9**, 265–270 (2018).
[58]A. Catenaccio, Y. Daruich, and C. Magallanes, "Temperature dependence of the permittivity of water," Chem. Phys. Lett. **367**(5–6), 669–671 (2003).